A Microscopic Study of One-Dimensional Solid ^{4}He Using the Static Fluctuation Approximation

E.M. Alhami[a], M.K. Al-Sugheir[b,*] and H.B. Ghassib[c]
[a]College of Education — Zulfi, Majmaah University, Saudi Arabia
[b]Department of Physics, Faculty of Science, The Hashemite University, Zarqa, Jordan
[c]Department of Physics, The University of Jordan, Amman, Jordan

(Received November 20, 2014)

In this work, solid helium is studied within the framework of the static fluctuation approximation. The closed set of nonlinear coupled equations, which is an inherent feature of this approximation, is derived for one-dimensional solid ^{4}He. This set is solved numerically by an iteration method for a realistic interhelium potential. The central aim is to determine the chemical potential μ, condensate fraction N_0/N, total energy U, heat capacity C, and entropy S of the system. The effects of temperature T, total number of particles N, frequency ω and lattice constant R on these properties are emphasized and explained. Below 80 mK: (1) as N or ω increases, μ increases; (2) as N increases, U, C, and S increase; whereas N_0/N, U/N, $C/Nk_{\rm B}$ and $S/Nk_{\rm B}$ decrease ($k_{\rm B}$ being Boltzmann's constant); (3) as ω increases, N_0/N, U, C, and S increase; whereas U/N, $C/Nk_{\rm B}$ and $S/Nk_{\rm B}$ are hardly affected; and (4) as $T \to 0$, the effect of R on N_0/N increases. These results are presented in a set of figures.

DOI: 10.12693/APhysPolA.127.1648
PACS: 67.80.B–, 67.25.de, 67.10.Ba

1. Introduction

Helium is a fascinating element, in all its phases and isotopic manifestations. Thanks to its light atomic mass, hence its large zero-point energy, and to the relatively weak (Van der Waals') attractive tail of the interhelium potential, helium remains liquid down to the lowest attainable temperatures; it is a "permanent" liquid. The solid phase can be produced only if a large external pressure is applied (about 25 atm for ^{4}He and 30 atm for ^{3}He, at 0 K). Solid helium forms a quantum crystal that cannot be treated by the classical theory of lattice dynamics. Its density is much lower than expected for the analogous classical system; hence the large compressibility of solid ^{4}He and solid ^{3}He [1].

Experimental work has focused on the thermodynamic properties of solid ^{4}He; in particular, its specific heat [2–6]. A peak in the specific heat has been reported below 200 mK, using a sample cell made of silicon, whose heat capacity is more than ten times lower than that of solid ^{4}He in the temperature range considered [4, 5]. Other accurate measurements [6] have confirmed this result. The presence of different concentrations of ^{3}He have not altered the position of the peak, which is around 75 mK. This also depends on the growth method, solids grown by the blocked-capillary method having a sharper peak [5].

Other experimental work has explored the extraordinary properties of solid helium such as the Bose–Einstein condensation (BEC) and possibly supersolidity [7–14]. Torsional-oscillator measurements have indicated that there is a reduction in the resonant period of the oscillator for solid ^{4}He [15–18]. This has been interpreted to have arisen from a reduction in the nonclassical rotational inertia.

Neutron-scattering measurements of the atomic distribution $n(k)$ were undertaken for three-dimensional solid helium under a pressure of 41 bar, with a molar volume of 20 cm^3/mol and at $T < 500$ mK [19]. The aim was to determine whether there was BEC below the temperature $T_0 = 200$ mK. It was found that the condensate fraction N_0/N was around 1%, and that the shape of $n(k)$ did not change on crossing T_0, within experimental errors. However, near the solidification pressure of 25.3 bar, neutron-scattering results indicated that the condensate was about 3% at the liquid/solid interface [20]. Very recently [21], extrapolation from liquid to solid densities suggested that $N_0/N \leq 1\%$ in the solid regime, assuming a frozen-liquid structure similar to an amorphous solid.

On the other hand, theoretical work has focused on the thermodynamic properties of solid helium, including the ground-state energy, pressure, compressibility and specific heat [1, 22–31]. A modified Brueckner theory was used to calculate the ground-state energy, pressure and compressibility of solid ^{3}He and ^{4}He with fcc structure [23]. The calculations were done for two different two-body potentials. The possibility of a phase transition to a metallic state at very high densities was considered. The ground-state energy and pressure for metallic helium were calculated, and the phase transition was found to occur at a pressure of about 2×10^7 atm.

Other theoretical work has drawn attention to the extraordinary properties of three-dimensional solid ^{4}He [29, 32–39]. It was proposed that when the quantum effects were large enough, the ground state might contain lattice defects, such as vacancies, which were delocalized and acted like a dilute Bose gas undergoing a BEC-transition [40]. Recently, Fil and Shevchenko [41]

*corresponding author; e-mail: msugh@hu.edu.jo

considered BEC of vacancies in a three-dimensional lattice. They showed that the critical temperature of BEC decreased with increasing length of the network segments.

The present work aims at deriving and calculating the thermodynamic properties of finite one-dimensional solid ^{4}He from the properties of its microscopic constituents, using the static fluctuation approximation (SFA). In particular, the chemical potential, condensate fraction, total energy, heat capacity and entropy will be computed. For this purpose, a system of N interacting ^{4}He atoms is considered, each atom vibrating about its site in the lattice. The total number of particles N, the frequency ω and the lattice constant R range from 500 to 2000, 10^6 to 10^7 Hz and 3 to 4 Å, respectively. The single-particle wave functions are taken to be the Hermite polynomials. The potential is chosen as the HFDHE2 of Aziz et al. [42] in its most recent version [43].

The main idea of SFA is to replace the square of the local-field operator with its mean value. The underlying physical meaning is that the quantum-mechanical spectrum of this operator is replaced with a distribution around its mean value [44]. In this work, SFA is used to explore the properties of one-dimensional solid ^{4}He, with special emphasis on the effects of dimensionality.

SFA has been used to study several many-body systems, ranging from the weakly- to the strongly-interacting [44–57]. It is relatively simple, compared to other many-body approaches. It has been found from numerous calculations over the years that SFA is more reliable for dilute and weakly-interacting systems or at low temperatures. The fluctuations in the local-field operator increase with increasing temperature or potential strength, thereby making SFA assumptions less realistic in these cases. However, SFA is still valid for strongly-interacting systems at low enough temperatures.

The rest of this paper is organized as follows. In Sect. 2, the SFA formalism for finite one-dimensional solid ^{4}He is derived, the principal aim being to obtain the corresponding closed set of nonlinear coupled equations of the system. In Sect. 3, the thermodynamic properties of the system are calculated using an algorithmic version of our formalism. Finally, in Sect. 4, the paper is closed with some concluding remarks.

2. Formalism

A one-dimensional chain of ^{4}He atoms is considered. The atoms at different lattice sites vibrate harmonically around their equilibrium positions, interacting with each other via a central potential. This is chosen as the HFDHE2 potential of Aziz et al. [42].

The single-particle wave functions for the system are taken to be Hermite polynomials $H_n(x)$ [58]:

$$\varphi_n(r) = \frac{\alpha^{1/4}}{\pi^{1/4}\sqrt{2^n n!}} \exp\left(-\frac{\alpha}{2}r^2\right) H_n\left(\sqrt{\alpha}r\right), \qquad (1)$$

with $\alpha = m\omega/\hbar$; the coordinates are measured from the equilibrium position. The total Hamiltonian can be written in second quantization as the sum of two terms

$$\hat{H} = \sum_{k=0}^{\infty} \hbar\omega \left(k + \frac{1}{2}\right) \hat{b}_k^+ \hat{b}_k + \hat{H}_1, \qquad (2)$$

the first being the harmonic term and the second the two-body interaction

$$\hat{H}_1 = \frac{1}{2} \iint \mathrm{d}r_1 \mathrm{d}r_2 \, \hat{\Psi}^+(r_1) \hat{\Psi}^+(r_2) V\left(|r_1 - r_2|\right) \times \hat{\Psi}(r_2) \hat{\Psi}(r_1), \qquad (3)$$

where $\hat{\Psi}(r)$ and $\hat{\Psi}^+(r)$ are the bosonic field operators and $V\left(|r_1 - r_2|\right)$ is the pairwise potential. In this work, only the first nearest-neighbor interaction is taken into account; the first atom is assumed to be at r_1 relative to its equilibrium position, and the second at r_2 relative to this position. It is then convenient to write the field operators for the first and second atoms as

$$\hat{\Psi}(r) = \sum_k \varphi_k(r) \hat{b}_k \text{ and } \hat{\Psi}(r_2) = \sum_k \varphi_k(r_2 - R) \hat{b}_k, \qquad (4)$$

R being the lattice constant. Based on the above, the total Hamiltonian can be written in second quantization as

$$\hat{H} = \sum_{k=0}^{\infty} \hbar\omega \left(k + \frac{1}{2}\right) \hat{b}_k^+ \hat{b}_k + \frac{1}{2} \sum_{n,m,p,q} C(n,m,p,q) \hat{b}_n^+ \hat{b}_m^+ \hat{b}_p \hat{b}_q, \qquad (5)$$

where

$$C(n,m,p,q) = \iint \mathrm{d}r_1 \mathrm{d}r_2 \varphi_n(r_1) \varphi_m(r_2 - R) \times V\left(|r_1 - r_2|\right) \varphi_p(r_2 - R) \varphi_q(r_1). \qquad (6)$$

SFA assumes that the total Hamiltonian can be written as a linear combination of a local-field operator $\hat{E}_k(\tau)$ and the occupation-number operator $\hat{n}_k = \hat{b}_k^+ \hat{b}_k$ [44]:

$$\hat{H} = \sum_{k=0}^{\infty} \hat{E}_k \hat{n}_k. \qquad (7)$$

Then

$$\hat{E}_k = \left[\hat{b}_k, \left[\hat{H}, \hat{b}_k^+\right]\right] = \hbar\omega \left(k + \frac{1}{2}\right) + \frac{1}{2} \sum_{m=0}^{\infty} F(k,m) \hat{n}_m, \qquad (8)$$

where

$$F(k,m) = 2C(m,k,m,k) + C(m,k,k,m) + C(k,m,k,m). \qquad (9)$$

The well-known mean-field approximation or the Hartree model states that $\hat{E}_k$ can be replaced with its mean value $\left\langle \hat{E}_k \right\rangle$; it assumes that the fluctuations φ_k in this operator are negligible. On the other hand, in SFA, the fluctuations are taken into account as well as the correlations between the fluctuations in the numbers of particles in different states. Accordingly, the local-field operator is defined as:

$$\hat{E}_k \equiv \left\langle \hat{E}_k \right\rangle + \Delta\hat{E}_k, \qquad (10)$$

$\Delta\hat{E}_k$ being the energy-fluctuations operator. The fluctuations in energy arise from the interactions between particles. It is straightforward to show that

$$\Delta\hat{E}_k = \frac{1}{2}\sum_{p=0}^{\infty} F(k,p)\Delta\hat{n}_p. \tag{11}$$

SFA assumes that the *square* of the local-field operator $\Delta\hat{E}_k(\tau)$ can be replaced with its mean value

$$\left(\Delta\hat{E}_k\right)^2 \cong \left\langle\left(\Delta\hat{E}_k\right)^2\right\rangle \equiv \phi_k^2. \tag{12}$$

This equation implies that $\Delta\hat{E}_k(\tau)$ has only two characteristic values: $\pm\phi_k$, where $\tau \equiv it$.

The generating equation based on SFA, as derived in [44], is given by

$$\left\langle\hat{n}_k\hat{A}\right\rangle = \eta_0(k)\left\langle\hat{A}\right\rangle + \eta_1(k)\left\langle\Delta\hat{E}_k\hat{A}\right\rangle, \tag{13}$$

$$\eta_0(k) \equiv \frac{1}{2}\left(\frac{1}{\exp\left(\beta\left(\left\langle\hat{E}_k\right\rangle - \mu + \phi_k\right)\right) - 1}\right.$$
$$\left. + \frac{1}{\exp\left(\beta\left(\left\langle\hat{E}_k\right\rangle - \mu - \phi_k\right)\right) - 1}\right), \tag{14}$$

$$\eta_1(k) \equiv \frac{1}{2\phi_k}\left(\frac{1}{\exp\left(\beta\left(\left\langle\hat{E}_k\right\rangle - \mu + \phi_k\right)\right) - 1}\right.$$
$$\left. - \frac{1}{\exp\left\{\beta\left(\left\langle\hat{E}_k\right\rangle - \mu - \phi_k\right)\right\} - 1}\right). \tag{15}$$

Putting $\hat{A} = 1$ in Eq. (13), we have

$$\langle\hat{n}_k\rangle = \eta_0(k) + \eta_1(k)\left\langle\Delta\hat{E}_k\right\rangle. \tag{16}$$

Using the fact that the quadratic fluctuations are symmetric, i.e., $\left\langle\Delta\hat{E}_k\right\rangle = 0$, we obtain for the particle distribution

$$\langle\hat{n}_k\rangle = \eta_0(k). \tag{17}$$

From the generating equation, the pair correlation function $\langle\Delta\hat{n}_k\Delta\hat{n}_q\rangle_{\rm c}$, for $k \neq q$, and the fluctuations in the local field operator, ϕ_k, can be calculated as

$$\langle\Delta\hat{n}_k\Delta\hat{n}_q\rangle_{\rm c} = \eta_1(k)\left\langle\Delta\hat{E}_k\Delta\hat{n}_q\right\rangle_{\rm c} =$$
$$\frac{\eta_1(k)}{2}\sum_{p=0}^{\infty} F(k,p)\langle\Delta\hat{n}_p\Delta\hat{n}_q\rangle, \tag{18}$$

$$\eta_1(k)\phi_k^2 = \frac{1}{2}F(k,k)\left\langle(\Delta\hat{n}_k)^2\right\rangle$$
$$+\frac{1}{2}\sum_{p=0}^{\infty} F(k,p)\langle\Delta\hat{n}_k\Delta\hat{n}_p\rangle_{\rm c}. \tag{19}$$

The quadratic fluctuations in the occupation numbers are given by [44]

$$\left\langle(\Delta\hat{n}_k)^2\right\rangle = \langle\hat{n}_k\rangle\left(1 + \langle\hat{n}_k\rangle\right)$$
$$+\eta_1(k)\sum_{p=0}^{\infty} F(k,p)\langle\Delta\hat{n}_p\Delta\hat{n}_k\rangle. \tag{20}$$

From the closed system of nonlinear coupled Eqs. (17)–(20), one can find $\langle\hat{n}_k\rangle$, $\left\langle(\Delta\hat{n}_k)^2\right\rangle$, $\langle\Delta\hat{n}_k\Delta\hat{n}_q\rangle_{\rm c}$, ϕ_k.

To calculate the thermodynamic properties of the system, the grand partition function Q should be derived. We start from the usual expression

$$Q{=}{\rm Tr}\left(\exp(-\beta\hat{H})\right) = \sum_{n_p}\exp\left(-\beta\sum_p\left(\hat{E}_p - \mu\right)\hat{n}_p\right) =$$
$$\prod_p\sum_{n_p}\exp\left(-\beta\left(\hat{E}_p - \mu\right)\hat{n}_p\right). \tag{21}$$

Hence,

$$\ln Q = -\frac{1}{2}\sum_p \ln\left(1 - 2\exp\left(-\beta\left(\left\langle\hat{E}_p\right\rangle - \mu\right)\right)\right.$$
$$\left.\times\cosh\left(\beta\phi_p\right) + \exp\left(-2\beta\left(\left\langle\hat{E}_p\right\rangle - \mu\right)\right)\right). \tag{22}$$

It follows that the grand internal energy U (the internal energy incorporating μ) is

$$U \equiv \left\langle\hat{H}\right\rangle = -\frac{\partial\ln Q}{\partial\beta} = \sum_{\boldsymbol{p}}\left\langle\hat{n}_p\left(\hat{E}_p - \mu\right)\right\rangle =$$
$$\sum_{\boldsymbol{p}}\left[\langle\hat{n}_p\rangle\left\langle\hat{E}_p - \mu\right\rangle + \phi_p^2\eta_1(p)\right]. \tag{23}$$

From Q and U, one can readily evaluate all other thermodynamic properties. Specifically, the heat capacity is

$$C = \left(\frac{\partial U}{\partial T}\right). \tag{24}$$

The entropy S is

$$S = \frac{U}{T} + k_{\rm B}\ln Q. \tag{25}$$

The closed set of coupled equations for two- and three-dimensional solid ^{4}He can be derived in exactly the same way as for one-dimensional solid ^{4}He. A suitable server could be used to solve this set in a reasonably short time. In this case, one could explore the effects of dimensionality on the properties of solid ^{4}He within SFA.

3. Results and discussion

In principle, the number of states m to be considered in solving the closed set of coupled equations should be infinity. In practice, however, this number is necessarily finite. A sufficiently large m should be chosen so as to make physical properties m-independent, as was discussed extensively in a previous work [51]; it was found that this m was T- and N-dependent. In this work, where N ranges from 500 to 2000 and T is below 80 mK, we found that the necessary number of states should be $m \approx 9000$; otherwise, unphysical behavior of the system sets in, especially at high T or large N.

The closed set of non-linear coupled equations was solved numerically by an iteration method. Our results are summarized in Figs. 1–15.

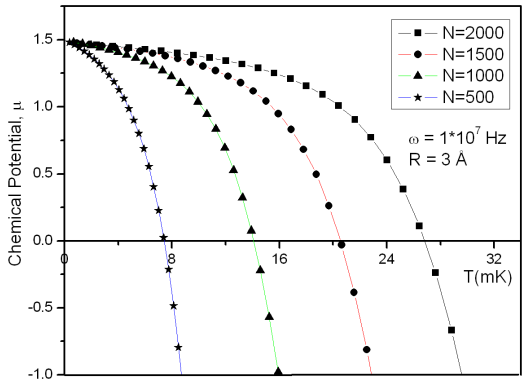

Fig. 1. The chemical potential μ in units of $\hbar\omega$ as a function of temperature T (in mK) for different total number of particles N. The frequency is $\omega = 10^7$ Hz, and the lattice constant is $R = 3$ Å.

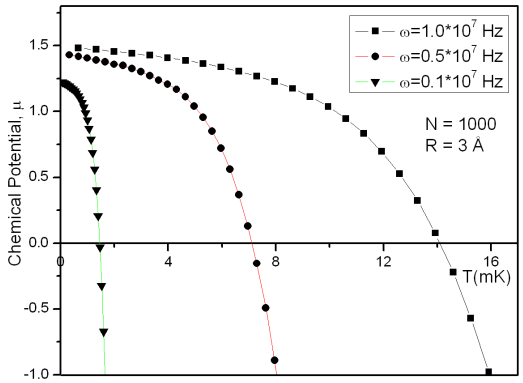

Fig. 2. The chemical potential μ in units of $\hbar\omega$ as a function of temperature T (in mK) for different values of frequency ω. The total number of particles is $N = 1000$, and the lattice constant is $R = 3$ Å.

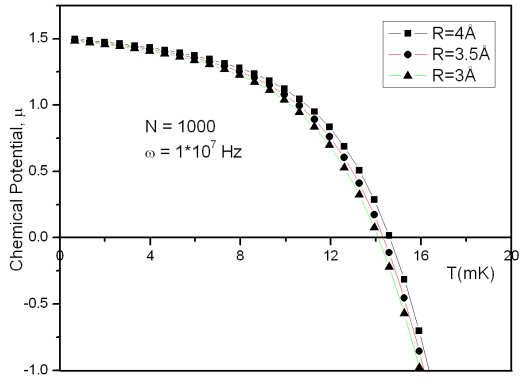

Fig. 3. The chemical potential μ in units of $\hbar\omega$ as a function of temperature T (in mK) for different values of lattice constant R. The total number of particles is $N = 1000$, and the frequency is $\omega = 10^7$ Hz.

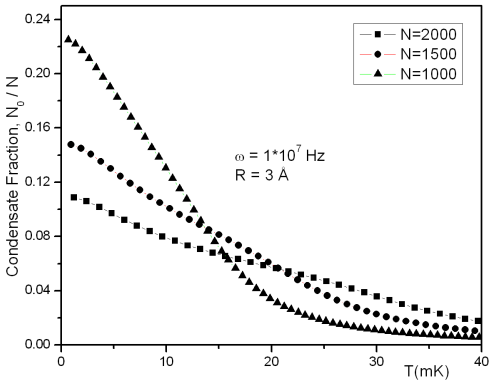

Fig. 4. The condensate fraction N_0/N as a function of temperature T (in mK) for different total number of particles N. The frequency is $\omega = 10^7$ Hz, and the lattice constant is $R = 3$ Å.

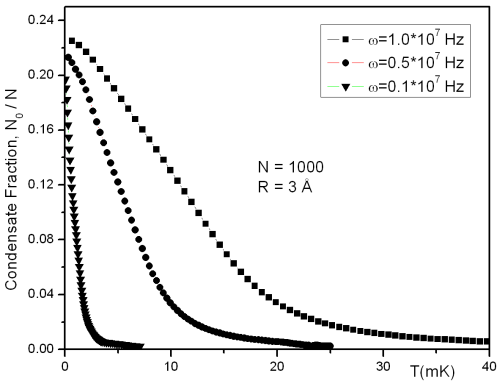

Fig. 5. The condensate fraction N_0/N as a function of temperature T (in mK) for different values of frequency ω. The total number of particles is $N = 1000$, and the lattice constant is $R = 3$ Å.

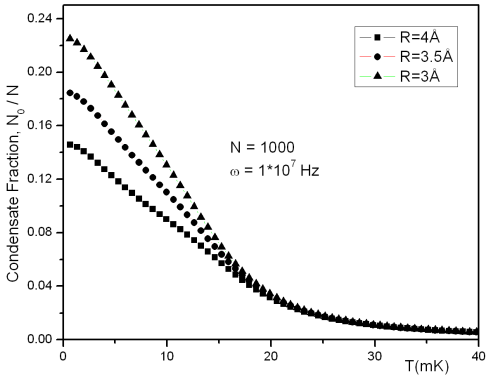

Fig. 6. The condensate fraction N_0/N as a function of temperature T (in mK) for different values of lattice constant R. The total number of particles is $N = 1000$, and the frequency is $\omega = 10^7$ Hz.

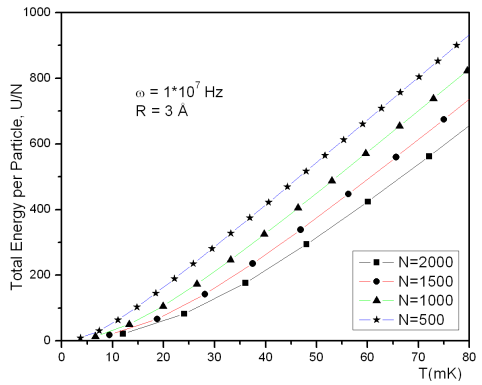

Fig. 7. The total energy per particle U/N in units of $\hbar\omega$ as a function of temperature T (in mK) for different total number of particles N. The frequency is $\omega = 10^7$ Hz, and the lattice constant is $R = 3$ Å.

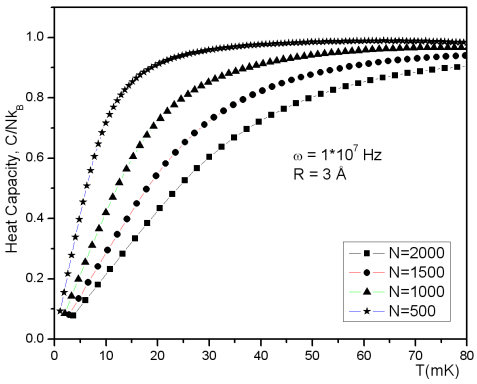

Fig. 10. The heat capacity $C/Nk_{\rm B}$ as a function of temperature T (in mK) for different total number of particles N. The frequency is $\omega = 10^7$ Hz, and the lattice constant is $R = 3$ Å.

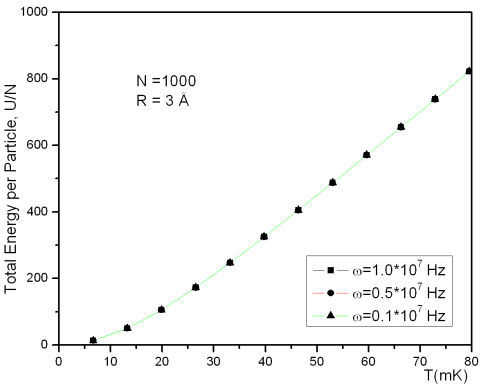

Fig. 8. The total energy per particle U/N in units of $\hbar\omega$ as a function of temperature T (in mK) for different values of frequency ω. The total number of particles is $N = 1000$, and the lattice constant is $R = 3$ Å.

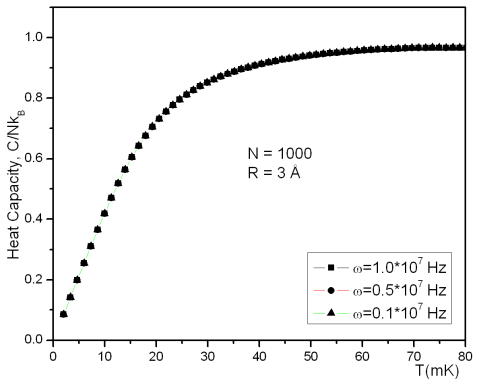

Fig. 11. The heat capacity $C/Nk_{\rm B}$ as a function of temperature T (in mK) for different values of frequency ω. The total number of particles is $N = 1000$, and the lattice constant is $R = 3$ Å.

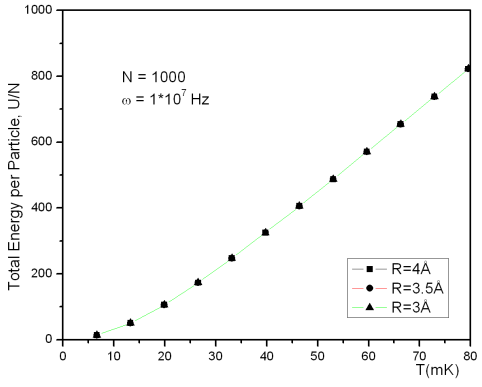

Fig. 9. The total energy per particle U/N in units of $\hbar\omega$ as a function of temperature T (in mK) for different values of lattice constant R. The total number of particles is $N = 1000$, and the frequency is $\omega = 10^7$ Hz.

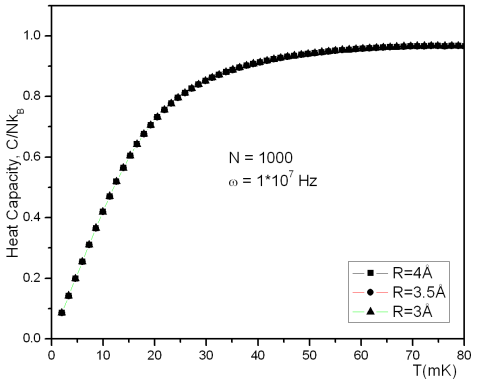

Fig. 12. The heat capacity $C/Nk_{\rm B}$ as a function of temperature T (in mK) for different values of lattice constant R. The total number of particles is $N = 1000$, and the frequency is $\omega = 10^7$ Hz.

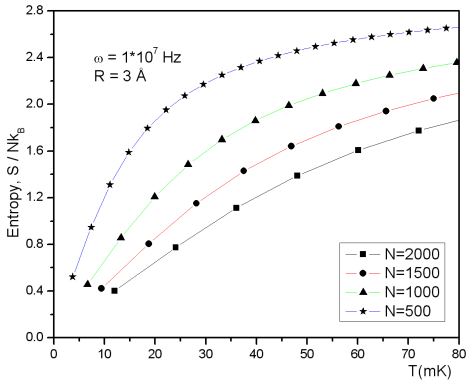

Fig. 13. The entropy $S/Nk_{\rm B}$ as a function of temperature T (in mK) for different total number of particles N. The frequency is $\omega = 10^7$ Hz, and the lattice constant is $R = 3$ Å.

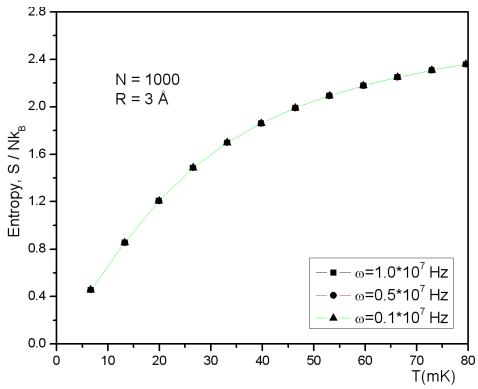

Fig. 14. The entropy $S/Nk_{\rm B}$ as a function of temperature T (in mK) for different values of frequency ω. The total number of particles is $N = 1000$, and the lattice constant is $R = 3$ Å.

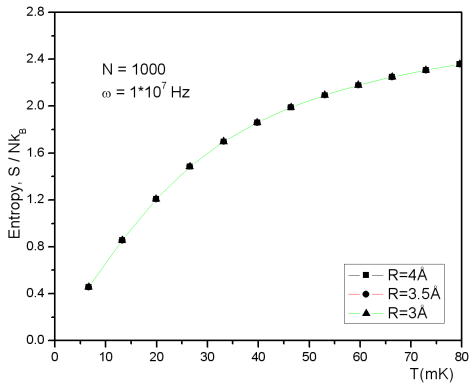

Fig. 15. The entropy $S/Nk_{\rm B}$ as a function of temperature T (in mK) for different values of lattice constant R. The total number of particles is $N = 1000$, and the frequency is $\omega = 10^7$ Hz.

3.1. Chemical potential

An open system was considered here, i.e., with a variable N. A well-known thermodynamic relation is [59–61]:

$$\mu = \left(\frac{\partial U}{\partial N}\right)_{S,V} = -T\left(\frac{\partial S}{\partial N}\right)_{U,V} . \tag{26}$$

For an *interacting* system, the calculation of μ is quite complicated, especially at high T. For such a system, the energy of the lowest-momentum state does not vanish, even at zero T. In this work, μ was calculated from the condition

$$N = \sum_k \langle n_k \rangle . \tag{27}$$

Our results for μ in units of $\hbar\omega$ are summarized in Figs. 1–3. These figures display μ as a function of T (in mK) for different N, ω, and R.

Figure 1 shows μ as a function of T for different N; $\omega = 10^7$ Hz and $R = 3$ Å. For all N, μ has the same behavior with T: it has the same maximum value at $T = 0$, then starts to decrease as T increases. As $T \to 0$, μ is essentially independent of N; whereas the dependence on N becomes more and more pronounced as T increases. Hence, as N increases, μ increases. This occurs because, as N increases, the interaction term in Eq. (8) increases since it depends on the numbers of particles in different states. Therefore, the transition from the quantum to the classical regime occurs at higher T as N increases.

Figure 2 represents μ as a function of T for different ω; $N = 1000$ and $R = 3$ Å. At $T = 0$, with ω increasing, the ground-state energy increases, as expected from Eq. (8); hence, μ shifts up to higher values. If T starts to increase, μ starts to decrease in all cases; but its variation with T is smaller for higher ω. Accordingly, μ decreases slower with T. Therefore, the transition from the quantum to the classical regime occurs at higher T as ω increases. Figure 3 displays μ as a function of T for different R; μ is almost independent of R in the range considered.

3.2. Condensate fraction

Our results for N_0/N are summarized in Figs. 4–6. These figures display N_0/N as a function of T for different N, ω, and R, respectively. The condensate represents the occupation number of particles in the state $m = 0$. At $T = 0$, the condensate has a maximum value (most particles occupy the state $m = 0$). As T starts to increase, the condensate begins to decrease monotonically until it vanishes in the classical limit.

Figure 4 shows N_0/N as a function of T for different N; $\omega = 10^7$ Hz and $R = 3$ Å. As N increases, N_0/N decreases; and so it does as T decreases. In *finite* (as distinct from infinite) one-dimensional Bose systems, condensation could take place. Figure 4 shows that N_0/N is appreciable for finite N at low T; however, it decreases with increasing N, as expected, going to zero in the limit $N \to \infty$. This is consistent with the well-known fact that in an *infinite* one-dimensional Bose system, no condensation occurs. However, experimental studies of (three-dimensional) solid He [19–21] have shown that the condensate, below 500 mK, is around 2%. The inconsistency

of our results with experiment arises from dimensionality; our system is one-, not three-dimensional.

Figure 5 shows N_0/N as a function of T for different ω; $N = 1000$ and $R = 3$ Å. The energy difference between successive states in the system increases as ω increases. Thus, at low T, as ω increases, an appreciable number of particles occupy the ground state.

Figure 6 displays N_0/N as a function of T for different R; $N = 1000$ and $\omega = 10^7$ Hz. The role of R here can be readily understood as soon as it is recalled that quantum effects set in when the interparticle spacing becomes comparable with the thermal de Broglie wavelength. Thus, as the lattice points come closer to each other (and, therefore R becomes smaller), the probability of BEC occurring becomes higher. Our results in Fig. 6 are consistent with this.

3.3. Total energy

Our results for the total energy per particle, U/N, are summarized in Figs. 7–9 in units of $\hbar\omega$. These figures display U/N as a function of T for different N, ω, and R.

Figure 7 shows U/N as a function of T for different N; $\omega = 10^7$ Hz and $R = 3$ Å. In the limit $T \to 0$, U/N is weakly-dependent on T and N. However, as T increases, the dependence of U/N on T and N becomes noticeable. These results can be explained as follows: At low T, regardless of N, most particles accumulate in the ground state. Thus, U/N will be a minimum and weakly-dependent on T. As T increases, more and more particles are excited to higher-energy states; hence, U and U/N increase. Figure 7 shows further that U/N has almost the same T-behavior for different N: it is almost proportional to T^2 at low T and is linear with T in the classical regime. Regardless of T, the interaction term in the energy spectrum, Eq. (8), depends on how the particles are distributed in the energy states as well as on N. As N increases, this term increases; hence, U increases, whereas U/N decreases. In addition, as T increases, this term increases and higher states become occupied. Energy is an extensive quantity *in the thermodynamic limit*; it is linearly-dependent on N, unlike U/N which is intensive. The "finiteness effect" is quite evident in our results: U/N is not intensive for our finite system. The difference in U/N at the same T between $N = 500$ and $N = 1000$ is greater than that between $N = 1500$ and $N = 2000$; this means that U/N-curves come closer to each other as N increases, U/N becoming intensive in the thermodynamic limit.

Figure 8 represents U/N in units of $\hbar\omega$ as a function of T for different ω; $N = 1000$ and $R = 3$ Å. Regardless of ω, U/N-curves are close to each other. This result means that the energy per particle is linearly-dependent on ω. Figure 9 displays U/N in units of $\hbar\omega$ as a function of T for different R; $N = 1000$ and $\omega = 10^7$ Hz. Clearly, U/N is independent of R. In the energy spectrum, Eq. (8), the "noninteraction" term is linearly-dependent on ω and is independent of R. The results presented in Figs. 8 and 9 indicate that the energy spectrum of the system is weakly-dependent on the interaction term.

3.4. Heat capacity

Our results for the heat capacity at constant "volume" C are summarized in Figs. 10–12. These figures display C/Nk_B as a function of T for different N, ω, and R.

Figure 10 shows C/Nk_B as a function of T for different N; $\omega = 10^7$ Hz and $R = 3$ Å. As N increases, C/Nk_B approaches the asymptotic value $(= 1)$ more slowly. In all cases, C/Nk_B increases monotonically until it reaches a plateau in the classical limit. The classical value for an infinite, noninteracting vibrating lattice in one dimension is $C/Nk_B = 1$. This indicates that at high T, the system behaves like a noninteracting vibrating lattice in one dimension. The transition from the quantum to the classical regime occurs at low T for small N: for $N = 500$, the system goes to the classical regime at $T \approx 20$ mK; whereas for $N = 1500$, the transition occurs at $T \approx 40$ mK. For large N, C/Nk_B almost "saturates" below one. This is presumably because of computational limitations; at high T and large N, m may well exceed 9000.

The specific heat capacity of three-dimensional solid ^{4}He was measured as a function of T below 200 mK [4, 6]. A peak was found. As the crystalline order increased, the magnitude of this peak decreased and its position shifted to higher T. In the present one-dimensional highly-crystalline solid, no peak exists.

Figure 11 represents C/Nk_B as a function of T for different ω; $N = 1000$ and $R = 3$ Å. It is ω-independent like U/N. Figure 12 shows C/Nk_B as a function of T for different R; $N = 1000$ and $\omega = 10^7$ Hz. As the energy of the system is weakly-dependent on R, so is C/Nk_B.

3.5. Entropy

Our results for the entropy S are summarized in Figs. 13–15. These display S/Nk_B as a function of T for different N, ω, and R. Figure 13 shows S/Nk_B as a function of T for different N; $\omega = 10^7$ Hz and $R = 3$ Å. As N increases, S/Nk_B decreases — as expected from the behavior of U/N and C/Nk_B. In the thermodynamic limit, S/N is an intensive quantity; but it is nonintensive for a finite system. As N increases, the S/Nk_B-curves become closer to each other than at small N.

Figure 14 represents S/Nk_B as a function of T for different ω; $N = 1000$ and $R = 3$ Å. The S/Nk_B-behavior is the same for all possible values of ω, just like U/N and C/Nk_B. Figure 15 shows S/Nk_B as a function of T for different R; $N = 1000$ and $\omega = 10^7$ Hz. As expected from the behavior of C/Nk_B and U/N, S/Nk_B is weakly-dependent on R.

4. Conclusion

In this work, the thermodynamic properties of finite one-dimensional solid ^{4}He were studied using the static fluctuation approximation. The set of nonlinear coupled equations involved was solved numerically by an iteration method for a realistic interhelium potential. The energy spectrum, the fluctuations in energy and in the number of atoms, the atomic distribution and the pair correlation function were computed and then used for determining the chemical potential, condensate fraction, total energy, heat capacity and entropy. The restriction to one dimension was dictated by computational limitations.

References

[1] O. Svorstøl, E. Østgaard, *Phys. Rev. B* **35**, 4713 (1987).

[2] J.M. Dundon, J.M. Goodkind, *Phys. Rev. Lett.* **32**, 1343 (1974).

[3] A.C. Clark, M.H.W. Chan, *J. Low Temp. Phys.* **138**, 853 (2005).

[4] X. Lin, A.C. Clark, M.H.W. Chan, *Nature* **449**, 1025 (2007).

[5] M.H.W. Chan, in: *Symp. on Quantum Phenomena and Devices at Low Temperatures*, Eds.: V. Eltsov, T. Heikkilä, Low Temperature Laboratory, Helsinki University of Technology, Helsinki 2008.

[6] X. Lin, A.C. Clark, Z.G. Cheng, M.H. Chan, *Phys. Rev. Lett.* **102**, 125302 (2009).

[7] A. Fraass, P.R. Granfors, R.O. Simmons, *Phys. Rev. B* **39**, 124 (1989).

[8] M.W. Meisel, *Physica B* **178**, 121 (1992).

[9] A.S. Rittner, J.D. Reppy, *Phys. Rev. Lett.* **101**, 155301 (2008).

[10] J. West, X. Lin, Z. Cheng, M.H.W. Chan, *Phys. Rev. Lett.* **102**, 185302 (2009).

[11] S. Balibar, *Nature* **464**, 176 (2010).

[12] M.W. Ray, R.B. Hallock, *Phys. Rev. Lett.* **105**, 145301 (2010).

[13] J.D. Reppy, *Phys. Rev. Lett.* **104**, 255301 (2010).

[14] S. Balibar, A.D. Fefferman, A. Haziot, X. Rojas, *J. Low-Temp. Phys.* **168**, 121 (2012).

[15] E. Kim, M.H.W. Chan, *Science* **305**, 1941 (2004).

[16] E. Kim, M.H.W. Chan, *J. Low-Temp. Phys.* **138**, 859 (2005).

[17] M. Kondo, S. Takada, Y. Shibayama, K. Shirahama, *J. Low-Temp. Phys.* **148**, 695 (2006).

[18] H. Choi, D. Takahashi, K. Kono, E. Kim, *Science* **330**, 1512 (2010).

[19] S.O. Diallo, J.V. Pearce, R.T. Azuah, O. Kirichek, J.W. Taylor, H.R. Glyde, *Phys. Rev. Lett.* **98**, 1 (2007).

[20] H.R. Glyde, S.O. Diallo, R.T. Azuah, O. Kirichek, J.W. Taylor, *Phys. Rev. B* **83**, 100507 (2011).

[21] H.R. Glyde, *J. Low-Temp. Phys.* **172**, 364 (2013).

[22] T.R. Koehler, *Phys. Rev. Lett.* **18**, 654 (1967).

[23] E. Østgaard, *Physica* **74**, 113 (1974).

[24] D.N. Loy, C.W. Woo, *Phys. Rev. B* **13**, 3790 (1976).

[25] O. Svorstøl, E. Østgaard, *Phys. Rev. B* **34**, 6192 (1986).

[26] D.M. Ceperley, *Rev. Mod. Phys.* **67**, 279 (1995).

[27] S. Moroni, F. Pederiva, S. Fantoni, M. Boninseqni, *Phys. Rev. Lett.* **84**, 2650 (2000).

[28] M.C. Adamska, P. Solma, J. Tomaszewski, *Phys. Status Solidi B* **240**, 55 (2003).

[29] J. Maris, S. Balibar, *J. Low-Temp. Phys.* **147**, 539 (2007).

[30] K.M. Khanna, T.W. Sakwa, L.S. Chelimo, Y.K. Ayodo, *Ind. J. Pure Appl. Phys.* **46**, 857 (2008).

[31] K.M. Khanna, Y.K. Ayodo, T.W. Sakwa, S.K. Rotich, P.K. Torongey, W.S. Mbugua, *Ind. J. Pure Appl. Phys.* **47**, 325 (2009).

[32] D.M. Ceperley, B. Bernu, *Phys. Rev. Lett.* **93**, 155303 (2004).

[33] M. Boninsegni, N.V. Prokof'ev, B.V. Svistunov, *Phys. Rev. E* **74**, 036701 (2006).

[34] B. Clark, D.M. Ceperley, *Phys. Rev. Lett.* **96**, 105302 (2006).

[35] L. Reatto, M. Rossi, D.E. Galli, *Int. J. Mod. Phys. B* **20**, 5081 (2006).

[36] L. Pollet, M. Boninsegni, A.B. Kuklov, N.V. Prokof'ev, B.V. Svistunov, M. Troyer, *Phys. Rev. Lett.* **98**, 135301 (2007).

[37] R. Rota, J. Boronat, *J. Low-Temp. Phys.* **162**, 146 (2011).

[38] R. Rota, Y. Lutsyshyn, C. Cazorla, J. Boronat, *J. Low-Temp. Phys.* **168**, 150 (2012).

[39] A.F. Andreev, I.M. Lifshitz, *Sov. Phys. JETP* **29**, 1107 (1969).

[40] G.V. Chester, *Phys. Rev. A* **2**, 256 (1970).

[41] D.V. Fil, S.I. Shevchenko, *J. Low-Temp. Phys.* **34**, 351 (2008).

[42] R.A. Aziz, V.P.S. Nain, J.S. Carley, W.L. Taylor, G.T. McConville, *J. Chem. Phys.* **70**, 4330 (1979).

[43] A.R. Janzen, R.A. Aziz, *J. Chem. Phys.* **103**, 2526 (1995).

[44] M.K. Al-Sugheir, H.B. Ghassib, R.R. Nigmatullin, *Int. J. Theor. Phys.* **40**, 1033 (2001).

[45] R.R. Nigmatullin, V.A. Toboev, *Theor. Math. Phys.* **80**, 94 (1989).

[46] R.R. Nigmatullin, A.A. Khamzin, H.B. Ghassib, *Solid State Commun.* **113**, 257 (2000).

[47] R.R. Nigmatullin, A.A. Khamzin, H.B. Ghassib, *Int. J. Theor. Phys.* **39**, 405 (2000).

[48] R.R. Nigmatullin, A.A. Khamzin, H.B. Ghassib, *Phys. Rev. E* **61**, 3441 (2000).

[49] M.K. Al-Sugheir, A.S. Sandouqa, B.R. Joudeh, S. Al-Omari, M. Awawdeh, F. Rawwagah, *Physica B* **405**, 2171 (2010).

[50] M.K. Al-Sugheir, H.B. Ghassib, M. Awawdeh, *Phys. Rev. A* **84**, 013617 (2011).

[51] M.K. Al-Sugheir, G. Alna'washi, H.B. Ghassib, A. Sandouqa, *Physica B* **407**, 2313 (2012).

[52] M.K. Al-Sugheir, H.B. Ghassib, *Int. J. Theor. Phys.* **41**, 705 (2002).

[53] M.K. Al-Sugheir, *Int. J. Theor. Phys.* **43**, 1527 (2004).

[54] B.R. Joudeh, M.K. Al-Sugheir, H.B. Ghassib, *Int. J. Mod. Phys. B* **19**, 3985 (2005).

[55] N.M. Ghulam, H.B. Ghassib, M.K. Al-Sugheir, *Phys. Rev. C* **75**, 064317 (2007).

[56] N.M. Ghulam, M.K. Al-Sugheir, H.B. Ghassib, *Int. J. Theor. Phys.* **47**, 2326 (2008).

[57] A.R. Sakhel, S.I. Qashou, R.R. Sakhel, H.B. Ghassib, *Phys. Rev. A* **82**, 063618 (2010).

[58] E. Merzbacher, *Quantum Mechanics*, 3rd ed., Wiley, New York 1998.

[59] R.K. Pathria, P.D. Beale, *Statistical Mechanics*, 3rd ed., Elsevier, Amsterdam 2011.

[60] G. Cook, R.H. Dickerson, *Am. J. Phys.* **63**, 737 (1995).

[61] R. Baierlein, *Am. J. Phys.* **69**, 423 (2001).